Walsh, C., Fisher, J., Spencer, R., Graham, D. W., Ashton, W. T., Brown, J. E., Brown, R. D., & Rogers, E. F. (1978) *Biochemistry 17*, 1942.
Whitesides, G., & San Filippo, J. (1970) *J. Am. Chem. Soc. 92*, 6611–24.
Wilkinson, K., & Williams, C., Jr. (1979a) *J. Biol. Chem. 254*, 852–62.
Wilkinson, K., & Williams, C., Jr. (1979b) *J. Biol. Chem. 254*, 862–71.
Williams, C. H. (1976) *Enzymes (3rd Ed.) 13*, 89.
Williams, C. H., Arscott, D. L., Matthews, R. G., Thorpe, C., & Wilkinson, K. D. (1979) *Methods Enzymol. 62D*, 185.
Williams, C. H., Arscott, D. L., & Schulz, G. (1982) *Proc. Natl. Acad. Sci. U.S.A. 79*, 2199.
Wilson, G. S. (1978) *Methods Enzymol. 54*, 396.
Zoller, M. J., & Smith, M. (1986) *Methods Enzymol. 100*, 468.
Zoller, M. J., & Smith, M. (1984) *DNA 3*, 479.

Mutagenesis of the N- and C-Terminal Cysteine Pairs of Tn*501* Mercuric Ion Reductase: Consequences for Bacterial Detoxification of Mercurials†

Melissa J. Moore and Christopher T. Walsh*
Department of Biological Chemistry and Molecular Pharmacology, Harvard Medical School, Boston, Massachusetts 02115
Received June 1, 1988; Revised Manuscript Received September 20, 1988

ABSTRACT: Mercuric ion reductase (the *merA* gene product) is a unique member of the class of FAD and redox-active disulfide-containing oxidoreductases by virtue of its ability to reduce Hg(II) to Hg(0) as the last step in bacterial detoxification of mercurials. In addition to the active site redox-active disulfide, formed between Cys_{135} and Cys_{140} in Tn*501* MerA, the protein products of the three *merA* gene sequences published to date have two additional conserved pairs of cysteines, one near the N-terminus ($Cys_{10}Cys_{13}$ in Tn*501* MerA) and another near the C-terminus ($Cys_{558}Cys_{559}$ in Tn*501* MerA). Neither of these pairs is found in other members of this enzyme family. To assess the possible roles of these peripheral cysteines in the Hg(II) detoxification pathway, we have constructed and characterized one single mutant, $Cys_{10}Ala_{13}$, and two double mutants, $Ala_{10}Ala_{13}$ and $Ala_{558}Ala_{559}$. The N-terminal mutants are fully functional in vivo as determined by $HgCl_2$ resistance studies, showing the N-terminal cysteine pair to be dispensable. In contrast, the $Ala_{558}Ala_{559}$ mutant is defective for $HgCl_2$ resistance in vivo and $Hg(SR)_2$ reduction in vitro, thereby implicating Cys_{558} and/or Cys_{559} in Hg(II) reduction by the wild-type enzyme. Other activities, such as NADPH/thio-$NADP^+$ transhydrogenation, NADPH oxidation, and DTNB reduction, are unimpaired in this mutant.

Mercuric reductase is the flavoenzyme that catalyzes the last and crucial step in Hg(II) detoxification by bacteria [for review see Foster (1983) and Summers (1986)]:[1]

$$Hg(SR)_2 + NADPH + H^+ \rightarrow Hg(0) + NADP^+ + 2HSR$$

It shows strong active site similarity to the disulfide oxidoreductases, pig heart lipoamide dehydrogenase, human glutathione reductase, and trypanothione reductase (Fox & Walsh, 1983; Shames et al., 1986), which catalyze the flow of electrons from NAD(P)H to disulfide substrates via a flavin coenzyme and an active site redox-active disulfide. However, while the three former proteins are all capable of binding mercurials in their two-electron-reduced states (Massey & Williams, 1965; Casola & Massey, 1966; Miller et al., 1986), only mercuric reductase is able to catalyze reduction of Hg(II) at a useful rate. In contrast, the physiological activities of both glutathione reductase and lipoamide dehydrogenase are potently inhibited by mercurials.

Tn*501* mercuric reductase is encoded by the *merA* gene of the *mer* operon in transposon Tn*501*, originally isolated on a plasmid from *Pseudomonas aeruginosa* (Stanisich et al., 1977). This operon is composed of a regulatory gene, *merR*, an operator/promoter region, and four structural genes: *merT*, *-P*, *-A*, and *-D*. *merT* and *merP* encode Hg(II)-transport and periplasmic Hg(II)-binding proteins, respectively, while no definitive function has yet been assigned to *merD*. A recurring structural motif throughout these *mer* gene products is the

Table I: Primary-Sequence Cysteine Pairs in the Tn*501* *mer* Operon

MerR[a]	113-LeuValCysAlaCysHisAla-119
MerT[b]	21-AlaSerAlaCysCysLeuGly-27
	76-CysLysProGlyGluValCys-82
MerP[b]	31-MetThrCysAlaAlaCysPro-37
MerA[c]	8-MetThrCysAspSerCysAla-14
	134-ThrCysValAsnValGlyCys-140
	555-GlnLeuSerCysCysAlaGly-561

[a] O'Halloran & Walsh, 1987. [b] Misra et al., 1984. [c] Brown et al., 1983.

† This work was supported in part by NIH Grant GM 216439. M.J.M. was the recipient of a National Science Foundation Predoctoral Fellowship.
* To whom correspondence should be addressed.

[1] Abbreviations: NADPH, reduced nicotinamide adenine dinucleotide phosphate; thio-$NADP^+$, thionicotinamide adenine dinucleotide phosphate; FAD, flavin adenine dinucleotide; DTNB, 5,5′-dithiobis(2-nitrobenzoate); TNB, 5-thio-2-nitrobenzoate dianion; EDTA, ethylenediaminetetraacetic acid; IPTG, isopropyl β-D-thiogalactopyranoside; bp, DNA base pair(s); SDS, sodium dodecyl sulfate; PAGE, polyacrylamide gel electrophoresis; HPLC, high-performance liquid chromatography; N or C terminal, proximal to the amino or carboxyl terminus of a protein; E_{ox}, EH_2, and EH_4, oxidized, two-electron-reduced, and four-electron-reduced forms, respectively, of mercuric reductase or of the disulfide oxidoreductases; K_{si}, inhibition constant for binding of a second substrate molecule to the enzyme–substrate complex.

0006-2960/89/0428-1183$01.50/0

primary sequence grouping of paired cysteines (Table I), a pair being defined as two cysteines separated by no more than five other amino acid residues. Because of the affinity of Hg(II) for bis-thiol ligation, it has been suggested that these cysteine pairs may play key roles in the detoxification pathway. The roles proposed include initial binding of Hg(II) in the periplasm, its transport through the cell membrane via specific transfer from one cysteine pair to the next, and its correct positioning in the active site of mercuric reductase for catalytic reduction (Brown, 1985).

Mercuric reductase itself has eight cysteines, six of which are paired. It is these three cysteine pairs, which are all conserved in the three mercuric reductases whose sequences have been published (Brown et al., 1983; Misra et al., 1985; Laddaga et al., 1987), that we have chosen as targets for site-directed mutagenesis. Using this method, we have previously shown that the $Cys_{135}Cys_{140}$ pair, which forms the active site redox-active disulfide of mercuric reductase, is essential for normal catalytic Hg(II) reduction (Schultz et al., 1985). The preceding paper (Distefano et al., 1989) describes further mutagenesis of the redox-active pair and the mechanistic implications of said mutants' behavior.

In this paper we report the directed mutagenesis of the N- and C-terminal cysteine pairs at positions 10, 13 and 558, 559, respectively. The most significant result of this work is the identification of the first structural element unique to mercuric reductase, i.e., unique among the disulfide oxidoreductases, that is essential for high levels of Hg(II) reductase activity. We report herein the in vivo and in vitro characterization of a double mutant of the C-terminal cysteine pair, $Ala_{558}Ala_{559}$. This mutant is catalytically impaired in $Hg(SR)_2$ reduction, yet retains wild-type levels of all other activities assayed, including NADPH/thio-$NADP^+$ transhydrogenation and aryl disulfide (DTNB) reduction. In the following paper (Miller et al., 1989) we build on these results to show that wild-type mercuric reductase actually has four cysteinyl thiols in its active site: Cys_{135}, Cys_{140}, Cys_{558}, and Cys_{559}. We also demonstrate that Cys_{558} and Cys_{559} are capable of forming a second, auxiliary disulfide whose reduction is a necessary priming step for optimal enzyme activity.

While the C-terminal cysteines are essential for Hg(II) reduction, it has previously been shown by in vitro proteolysis that the 85 amino acid, N-terminal domain of mercuric reductase is not involved in catalysis (Fox & Walsh, 1983). This, coupled with its homology to the *merP* gene product, led Brown (1985) to suggest that the N-terminal domain plays a role in intracellular Hg(II) transport via the $Cys_{10}Cys_{13}$ thiols. However, by in vivo characterization of both a single mutant, $Cys_{10}Ala_{13}$, and a double mutant, $Ala_{10}Ala_{13}$, of this pair we show here that these cysteines are not essential for Hg(II) detoxification. We also present the construction of a shortened form of the *merA* gene, *merAΔ85*, that should encode an enzyme that is the wild-type mercuric reductase minus its 85-residue N-terminal domain. Unfortunately, *merAΔ85* fails to produce significant levels of protein, and thus the function of the N-terminal domain, if any, remains a mystery.

Experimental Procedures

Materials

Escherichia coli strain CSH26 *recA* containing plasmid pUB3451 (a pJOE114 derivative with *Bam*HI linkers in the 5811 bp *Not*I site) was the generous gift of Dr. Nigel Brown of the Department of Biochemistry, University of Bristol, Bristol BS8 1TD, UK. *E. coli* strain JM101, which was used for mutagenesis and routine M13 manipulations, and M13 RF DNAs were obtained from New England Biolabs. *E. coli* strain RZ1032 (Kunkel, 1988), which was used as the *dut⁻ ung⁻* strain in later M13 mutageneses, was the kind gift of Dr. Thomas A. Kunkel. *E. coli* strain HB101*, a derivative of HB101 giving higher transformation frequencies, was used for all plasmid manipulations and was kindly provided by Dr. David Botstein, Department of Biology, MIT, Cambridge, MA. Plasmids pJOE114, pSE181, and pPSO1, M13 derivative M13ps1, and *E. coli* strain W3110 $lacI^q$ were described previously (Schultz et al., 1985). Yeast glutathione reductase, *Pseudomonas cepacia* protocatechuate reductase, and milk xanthine oxidase were gifts from Drs. Charles Williams, Jr., David Ballou, and Vincent Massey, respectively.

All restriction enzymes, T4 polynucleotide kinase, T4 DNA ligase, and DNA polymerase I large fragment (Klenow) for mutagenesis and plasmid constructions were obtained from New England Biolabs, calf intestinal phosphatase was from Boehringer-Mannheim, and avian reverse transcriptase was from Pharmacia. Unlabeled reagents and Klenow fragment for Sanger sequencing were from Amersham or Boehringer-Mannheim, while ^{32}P- and ^{35}S-labeled nucleotides and ^{35}S-labeled amino acids were purchased from Amersham or New England Nuclear. Protected mononucleotides for phosphotriester oligonucleotide synthesis were obtained from Biosearch. Orange A Matrex gel was purchased from Amicon Corp. and P6-DG desalting gel from Bio-Rad. All other reagents and chemicals were of the highest grade commercially available.

Methods

DNA Manipulations. All techniques used in M13 template construction, preparation, and Sanger sequencing are described in the *M13 Cloning and Sequencing Handbook* (Amersham, 1983) with the exception that uracil-containing M13 templates were prepared as described by Kunkel (1985). Transformations were performed according to the simple transformation protocol of Hanahan (1985). Reverse transcriptase sequencing of double-stranded plasmid DNA was as described by Seidmann (1986). All other cloning techniques and the Maxam–Gilbert sequencing protocol can be found in *Molecular Cloning: A Laboratory Manual* (Maniatis et al., 1982).

M13 Templates. The M13 template used for directed mutagenesis in the N-terminal portion (i.e., residues 1–186) of *merA*, M13ps1, has been described elsewhere (Schultz et al., 1985). A template containing the C-terminal region (i.e., residues 392–561) of *merA*, M13mm1, was constructed by inserting the 775 bp *Sph*I/*Bam*HI fragment of pUB3451 into *Sph*I/*Bam*HI-digested M13mp19 (see Figure 2). This insertion was confirmed by Sanger sequencing with universal primer.

Oligonucleotides. Oligonucleotides for both mutagenesis and sequencing were synthesized according to a modified phosphotriester procedure on a Biosearch *Sam*I automated DNA synthesizer and were purified by polyacrylamide gel electrophoresis (Biosearch, 1984).

Mutagenesis. (*A*) *$Cys_{10}Ala_{13}$ and $Ala_{10}Ala_{13}$.* The $Cys_{10}Ala_{13}$ mutation was generated in the M13 vector, M13ps1, with a 17-mer oligonucleotide, 5′-CGCCGCG*GC*CGAGTCGC-3′. M13ps1 containing this mutation, M13mma13, was subsequently used as the template for $Cys_{10}Ala_{13}$ to $Ala_{10}Ala_{13}$ mutagenesis via a second 17-mer, 5′-CGAGTCG*GC*AGTCATGC-3′, generating M13mma10a13. Both primers contained two mismatched base pairs (italicized), and a primer:template ratio of 30:1 was used in both mutagenesis mixtures. Mutagenesis reactions were carried out by using a two-primer modification of the standard Zoller and Smith (1983) procedure described by

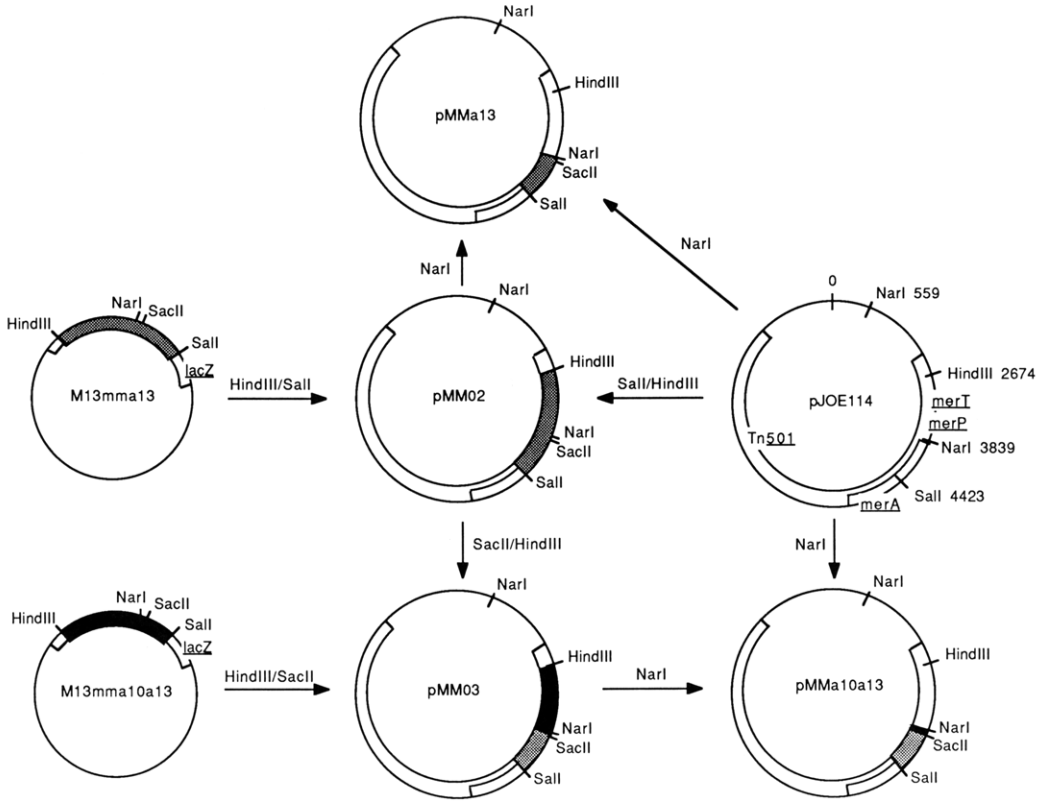

FIGURE 1: Construction of pJOE114 varients containing the Ala_{13} (pMMa13) and $Ala_{10}Ala_{13}$ (pMMa10a13) mutations in *merA*.

Messing (1983), except that the alkaline sucrose gradient centrifugation was omitted. Mutations were initially detected via hybridization screening of first-round phage isolates, followed by Sanger sequencing after a second round of phage growth.

By use of the above techniques the $Cys_{10}Ala_{13}$ and $Ala_{10}Ala_{13}$ mutations were obtained with 0.8% and 1.7% efficiencies, respectively. Unfortunately, in addition to the generation of the desired mutations in low yields, these mutageneses were also plagued with both spurious deletions of insert DNA and the production of undesired point mutations. The $Cys_{10}Cys_{13}$ to $Cys_{10}Ala_{13}$ mutagenesis reaction produced an additional point mutation in the *merT* gene, while the $Cys_{10}Ala_{13}$ to $Ala_{10}Ala_{13}$ mutagenesis yielded a 350 bp deletion in *merA* immediately 3′ to the Ala_{13} codon. The formation of these secondary mutations was probably exacerbated by both the large size of this M13 insert (1748 bp) and the high GC content [approximately 65% (Brown et al., 1983)] of the Tn*501 mer* operon. In order to remove these secondary mutations, both the $Cys_{10}Ala_{13}$ and $Ala_{10}Ala_{13}$ mutations were reconstructed into the *mer* operon of pJOE114 via the series of restriction fragment replacements described below (Figure 1).

(*B*) *M13mmΔ85 and M13mma558a559.* To increase mutagenesis efficiencies, both subsequent mutageneses (M13ps1 to M13mmΔ85 and M13mm1 to M13mma558a559) were carried out on templates that had been grown for two generations in the *dut⁻ ung⁻* strain RZ1032 (Kunkel, 1985, 1988). M13mmΔ85, in which *merA* residues 2–86 have been deleted, was generated from M13ps1 by using a 21-mer, 5′-GGCGGCGGCCATGCAACAGAT-3′, that primed at both ends of the desired deletion, causing the intervening DNA sequence to be looped out and lost. M13mma558a559 contains the $Ala_{558}Ala_{559}$ double mutation and was generated in one step from M13mm1 with a 20-mer, 5′-CCCGGCG*GCGGC*GGAAAGCT-3′, possessing four mismatched base pairs (italicized). Optimal primer:template ratios were determined to be 5:1 for the former primer with M13ps1 and 10:1 for the latter with M13mm1 by using the specific priming test via Sanger sequencing described by Zoller and Smith (1983). Mutagenesis reactions were performed as described by Kunkel (1985) except that uracil glycosylase treatment was omitted. These mutagenesis mixtures were used to transform JM101, and phage prepared from resulting plaques were screened for mutations directly by Sanger sequencing. According to this method the mutant M13 derivatives, M13mmΔ85 and M13mma558a559, were obtained in 12.5% and 16.7% yields, respectively. No secondary mutations were found to result from either of these mutageneses.

Plasmid Constructions. (*A*) *pMMa13.* The intact $Cys_{10}Ala_{13}$ *merA* gene was reconstructed in the *mer* operon (Figure 1) by first replacing the 1748 bp *Hin*dIII/*Sal*I fragment of pJOE114 with that of M13mma13. However, this plasmid, pMM02, contains an additional undesired mutation in *merT* (see above). Therefore, a pJOE114 derivative containing only the $Cys_{10}Ala_{13}$ *merA* mutation, pMMa13, was constructed by excising the *merT*-containing *Nar*I fragment of pMM02 and replacing it with the same fragment from wild-type pJOE114.

(*B*) *pMMa10a13.* The $Ala_{10}Ala_{13}$ *merA* gene was reconstructed by taking advantage of a *Sac*II site created by the Ala_{13} mutation. The 1236 bp *Hin*dIII/*Sac*II fragment of M13mma10a13 was cloned into *Hin*dIII/*Sac*II-digested pMM02. This was followed by replacement of the 3280 bp *Nar*I fragment with that of pJOE114 as described above to create pMMa10a13 (Figure 1). These manipulations ensured that only the 584 bp *Nar*I/*Sal*I fragments of pMMa13 and pMMa10a13 were ever present as single-stranded DNA that had undergone primer-mediated mutagenesis. To eliminate the possibility of any remaining secondary mutations, the sequences 50 bp to either side of the desired mutations were confirmed by double-stranded Maxam–Gilbert sequencing

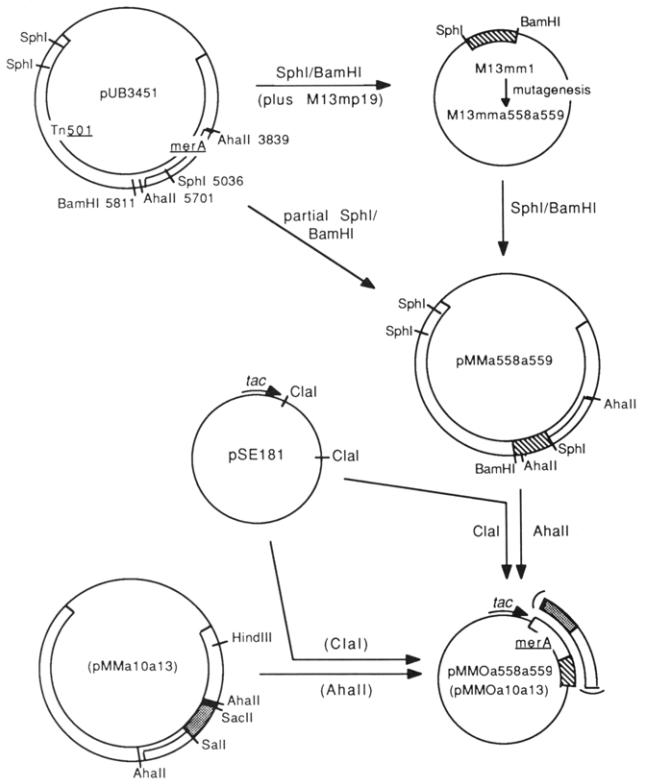

FIGURE 2: Construction of M13mm1 (C-terminal *merA* mutagenesis template), pMMa558a559 (pUB3451 containing the $Ala_{558}Ala_{559}$ mutation in *merA*), and the mutant MerA overproducing plasmids, pMMOa558a559 and pMMOa10a13. pMMOa10a13 construction and its insert into pSE181 are shown in parentheses.

from the *Nar*I site at bp position 3839 of both plasmids. Additionally, the 566 bp *Xho*II/*Sal*I fragment of pMMa13 was subcloned into *Bam*HI/*Sal*I-digested M13mp18 (not pictured) and Sanger sequenced in its entirety. (The same fragment of pMMa10a13 was derived from pMM02, the precursor to pMMa13, during plasmid reconstruction as described above, eliminating the necessity to similarly resequence it.)

(*C*) *pMMΔ85 and pMMa558a559.* pMMΔ85 was constructed by inserting the 329 bp *Nar*I/*Sal*I fragment of M13mmΔ85 into the 11 490 bp *Sal*I/*Nar*I fragment of pJOE114 generated by complete digestion with *Sal*I and partial digestion with *Nar*I (not pictured). pMMa558a559 was constructed by ligating the 775 bp *Sph*I/*Bam*HI fragment of M13mma558a559 with the 11 299 bp pUB3451 fragment generated by complete digestion with *Bam*HI and partial digestion with *Sph*I (Figure 2). Both pMMΔ85 and pMMa558a559 were confirmed by restriction mapping and Maxam–Gilbert or reverse transcriptase sequencing in the area of the desired mutation, and as above, the *Xho*II/*Sal*I pMMΔ85 fragment and the *Sph*I/*Bam*HI pMMa558a559 fragment were subcloned back into M13 and completely resequenced (not pictured).

(*D*) *pMMOa558a559 and pMMOa10a13.* *Tac*-based overproducers of the $Ala_{558}Ala_{559}$ and $Ala_{10}Ala_{13}$ mutant mercuric reductases were constructed by cloning the 1861 bp *Aha*II fragment of pMMa558a559 or pMMa10a13, respectively, into *Cla*I-digested pSE181 (Figure 2). These constructions, pMMOa558a559 and pMMOa10a13, were screened for insert directionality by restriction mapping and for their ability to produce bands of the correct molecular mass by SDS–PAGE after induction with IPTG in strain W3110 $lacI^q$. pMMOa558a559 was used to overproduce $Ala_{558}Ala_{559}$ mercuric reductase as described below, while pMMOa10a13 was used to generate $Ala_{10}Ala_{13}$ enzyme as presented in the following paper (Miller et al., 1989).

Growth Curves. Klett units of turbidity were measured on a Klett colorimeter with a No. 808 red filter. HB101* cells containing the appropriate plasmid were cultured overnight at 37 °C in amp^+ 2 × YT medium. These cultures were diluted 1:100 into amp^+ 2 × YT medium and grown to approximately 35 Klett units. The cultures were then divided, varying concentrations of $HgCl_2$ were added, and growth was monitored by taking Klett measurements every 30 min for a total of $7^1/_2$ h (Nakahara et al., 1979b).

Pulse Labeling of $HgCl_2$-Induced Proteins. HB101* cells transformed with either pMMΔ85 or pMMa558a559 were cultured in supplemented M9 minimal medium (20 μg/mL thiamine hydrochloride, 0.1% each of the L-amino acids, excluding cysteine and methionine). At A_{550} = 0.43, the cultures were divided in half and 0.5 μM $HgCl_2$ was added to one half to induce *mer* operon translation. After a 15-min incubation period, [^{35}S]-L-methionine and [^{35}S]-L-cysteine were added to both induced and uninduced cultures to a final concentration of 10 μCi/mL each. One-milliliter samples were removed at 2, 5, 10, and 20 min after the addition of the radioactivity. The samples were quickly centrifuged, and the cell pellets were flash-frozen in dry ice/ethanol and stored at −70 °C. Total cellular protein was electrophoresed on a 5–20% polyacrylamide gradient SDS gel (Hames, 1981) and the dried gel exposed to film overnight. Autoradiographs were scanned with an LKB UltroScan XL laser densitometer.

Protein Purification. Both the wild-type and $Ala_{558}Ala_{559}$ enzymes were purified from W3110 $lacI^q$/(pPSO1 or pMMOa558a559) cells as previously described (Schultz et al., 1985), with the following modifications: (a) the cells were induced at A_{595} = 0.7 by the addition of only 1 mM IPTG and were harvested $4^1/_2$–6 h thereafter; (b) no protease inhibitors were added to the purification buffer; (c) after enzyme elution from the Orange A column with 200 μM NADPH, the pooled fractions were incubated at 4 °C with excess FAD to ensure maximal loading of flavin. Excess FAD and NADPH were removed by passing samples through a Bio-Rad P6-DG desalting column. Enzyme samples were routinely stored at 4 °C in 20 mM sodium phosphate (pH 7.5), 0.5 mM EDTA, and 0.1% β-mercaptoethanol or at −70 °C after addition of glycerol to 15% (v/v).

Enzyme-bound $NADP^+$ was removed via exhaustive dialysis of enzyme against 2 M KBr (Fox & Walsh, 1982) in 20 mM sodium phosphate (pH 7.5) and 0.5 mM EDTA, followed by incubation with excess FAD and desalting on a P-6DG column as above, using the same buffer minus KBr. β-Mercaptoethanol was not added to KBr-dialyzed samples.

Spectrophotometry. UV/visible spectra and single-wavelength measurements were recorded on a Perkin-Elmer 554, a Perkin-Elmer Lambda 5 double-beam, or a Hewlett-Packard 8452A diode array spectrophotometer. Fluorescence spectra were recorded at 2–4 °C by Dr. Vincent Massey, Department of Biological Chemistry, University of Michigan, Ann Arbor, MI. Other fluorescence measurements were made with a Perkin-Elmer LS-3 fluorometer at ambient temperature.

Enzyme Concentrations. For activity measurements and thiol titrations, enzyme concentrations were based on flavin content, using an extinction coefficient of 11.3 mM^{-1} cm^{-1} at 456 nm for both the wild-type and $Ala_{558}Ala_{559}$ enzymes. Thiol titrations were only performed on enzyme samples with an A_{272}/A_{456} spectral ratio less than 6.5, ensuring that the flavin concentration truly reflected the concentration of protein monomer.

Physical Characterization. The extinction coefficient for flavin in the $Ala_{558}Ala_{559}$ mutant was determined by liberating FAD from the enzyme with heat in 10 mM $MgCl_2$ as described by Schultz et al. (1985). Monomer protein molecular masses were established by SDS–PAGE, while native molecular masses were determined by gel filtration on a Waters HPLC equipped with a Bio-Rad 300 mm × 7.5 mm TSK 250 column and 75 mm × 7.5 mm TSK 250 guard column. Samples were run in 50 mM sodium sulfate and 20 mM sodium phosphate, pH 6.8, at 1.0 mL/min.

Thiol Titrations. β-Mercaptoethanol was removed from enzyme samples to be used for thiol titrations via a Bio-Rad P6-DG desalting column. Thiols were titrated in aerobic solutions with DTNB in 4–5 M guanidine hydrochloride as described previously by Fox and Walsh (1982) or in 6 M guanidine hydrochloride by the method of Riddles et al. (1983). Reduced enzyme samples were generated by addition of 200 μM NADPH (25 °C) and were then denatured with guanidine hydrochloride within 1 min of this addition. An extinction coefficient of 13.7 mM^{-1} cm^{-1} at 412 nm was used for TNB in 6 M guanidine hydrochloride (Riddles et al., 1983).

Anaerobic Redox Titrations. Anaerobic enzyme titrations with NADPH and dithionite were performed as described elsewhere (Miller et al., 1989; Fox & Walsh, 1982) in double-side-armed anaerobic cuvettes similar to those of Williams et al. (1979). Enzyme samples were made anaerobic by repeated cycles of evacuation and flushing with argon that had been passed through an oxygen-absorbing cartridge. Dithionite solutions were standardized anaerobically against riboflavin both before and after each set of enzyme titrations.

Redox Potentials. Midpoint potentials for the E_{ox}/EH_2 and EH_2/EH_4 enzyme couples were determined by spectrophotometrically following the reduction of KBr-dialyzed enzyme, with a coupled xanthine/xanthine oxidase system as the reductant, in the presence of an appropriate indicator redox dye. ($NADP^+$-free enzyme samples are used to avoid unnecessary complications from both the free and enzyme-bound $NADP^+$/NADPH couples.) This method will be described in detail elsewhere [V. Massey et al., unpublished results; see also footnote 2, Distefano et al. (1989)]. The $Ala_{558}Ala_{559}$ E_{ox}/EH_2 potential was established in 100 mM sodium phosphate (pH 7.5) with the redox dye 1-deazariboflavin [$E^{\circ\prime}$ = −280 mV (Walsh et al., 1979)], while its EH_2/EH_4 potential was determined with benzylviologen [$E^{\circ\prime}$ = −358 mV (Wilson, 1978)] in 100 mM sodium phosphate (pH 7.0). Concentrations of oxidized and reduced species and the midpoint potentials were calculated in the same manner as that described by Fox and Walsh (1982).

Enzyme Assays. (*A*) *Aerobic.* $Hg(SR)_2$-independent and $Hg(SR)_2$-dependent NADPH oxidation assays were performed aerobically at 37 °C in 80 mM sodium phosphate (pH 7.4), 200 μM NADPH, and 1 mM β-mercaptoethanol. NADPH consumption was monitored at 340 nm (absorbance), and O_2 consumption rates were measured with a Yellow Springs Instrument Co. biological oxygen monitor (Model 53). Thio-$NADP^+$-dependent NADPH oxidation was monitored at ambient temperature in 80 mM sodium phosphate (pH 7.4), 1 mM β-mercaptoethanol, and 100 μM thio-$NADP^+$ by either NADPH absorbance at 340 nm or fluorescence emission at 470 nm (excitation at 340 nm). Transhydrogenase rates in crude extracts were measured similarly with 200 μM NADPH at 25 °C.

(*B*) *Anaerobic.* DTNB reduction rates were determined in anaerobic solutions that were prepared in a helium atmosphere glovebox and then sealed in stoppered test tubes. TNB production was monitored at 412 nm (ϵ = 13.7 mM^{-1} cm^{-1}) or at 440 nm (ϵ = 9.6 mM^{-1} cm^{-1}) with assays carried out in 80 mM sodium phosphate (pH 7.4) and 200 μM NADPH (25 °C).

$^{203}Hg(0)$ volatilization assays were carried out in 10-mL Wheaton vials as described by Distefano et al. (1989) except that reaction mixtures contained 100 μM $HgCl_2$, 1 mM cysteine, and 400 μM NADPH in 100 mM sodium phosphate (pH 7.4). To ensure anaerobiosis, assay mixtures containing all components (except $^{203}HgCl_2$) were incubated for 1 h (37 °C) with protocatechuate and protocatechuate dioxygenase. Reactions were then initiated by adding anaerobic $^{203}HgCl_2$, and its volatilization was monitored as described. The specific activity of the yeast glutathione reductase sample used for $^{203}Hg(0)$ volatilizations was checked according to the conditions given by Massey and Williams (1965).

Results

Growth Curves. The three mutations in the N-terminus of Tn*501* mercuric reductase ($Cys_{10}Ala_{13}$, $Ala_{10}Ala_{13}$, and *merAΔ85*) were created to test the hypothesis that the N-terminal domain is involved in Hg(II) transport via the Cys_{10} and Cys_{13} thiols. However, since none of these mutations was expected to affect the enzyme's catalytic properties (see Discussion), the consequences of each (as well as the $Ala_{558}Ala_{559}$ mutation) were first assessed by examining its in vivo effect on the $HgCl_2$ resistance phenotype.

Resistance phenotypes were determined by challenging HB101* cells containing each mutant *mer* operon with various concentrations of $HgCl_2$ and following their subsequent growth in liquid medium (Nakahara et al., 1979b). As can be seen in Figure 3, this method allows the distinction of three main phenotypic classes: $HgCl_2$ sensitive (Figure 3A), $HgCl_2$ supersensitive (Figure 3B), and $HgCl_2$ resistant (Figure 3C). $HgCl_2$-sensitive cells are those containing an ampicillin resistance determinant but no *mer* genes. These cells are able to grow in up to 25 μM $HgCl_2$ but are killed by 50 μM $HgCl_2$. Resistant cells contain a functionally intact *mer* operon. They show some slowing of growth at all $HgCl_2$ concentrations tested, probably due to amplified *mer* protein production from this multicopy plasmid system, but grow well even at 250 μM $HgCl_2$. Supersensitive cells are those that retain the specific Hg(II)-transport system but lack a functional mercuric reductase. These cells essentially commit suicide by concentrating Hg(II) in their cytoplasms and characteristically exhibit growth inhibition in $HgCl_2$ concentrations as low as 2.5 μM. Conversely, cells that have a working mercuric reductase, but are impaired in Hg(II) transport, have phenotypes very similar to Hg(II)-sensitive cells (not shown).

Under the conditions of this assay both pMMa13 (encoding $Cys_{10}Ala_{13}$ mercuric reductase) and pMMa10a13 ($Ala_{10}Ala_{13}$ mercuric reductase) are indistinguishable from wild-type pJOE114 in their conferred resistance (Figure 3C). This result indicates that at least in this gene-amplified system (see Discussion) neither Cys_{10} nor Cys_{13} is essential for Hg(II) transport as proposed. In sharp contrast, however, cells carrying either pMMΔ85 (encoding N-terminus-deleted mercuric reductase) or pMMa558a559 ($Ala_{558}Ala_{559}$ mercuric reductase) exhibit a $HgCl_2$-supersensitive phenotype (Figure 3B).

$HgCl_2$-Inducible Gene Products of pMMΔ85 and pMMa558a559. The observation that both pMMΔ85 and pMMa558a559 confer supersensitivity to $HgCl_2$ suggests that neither mutant *merA* gene encodes a catalytically functional mercuric reductase. Correspondingly, no $Hg(SR)_2$-dependent consumption of NADPH was observed in HB101 pMMΔ85 crude cell extracts after induction with subtoxic $HgCl_2$ con-

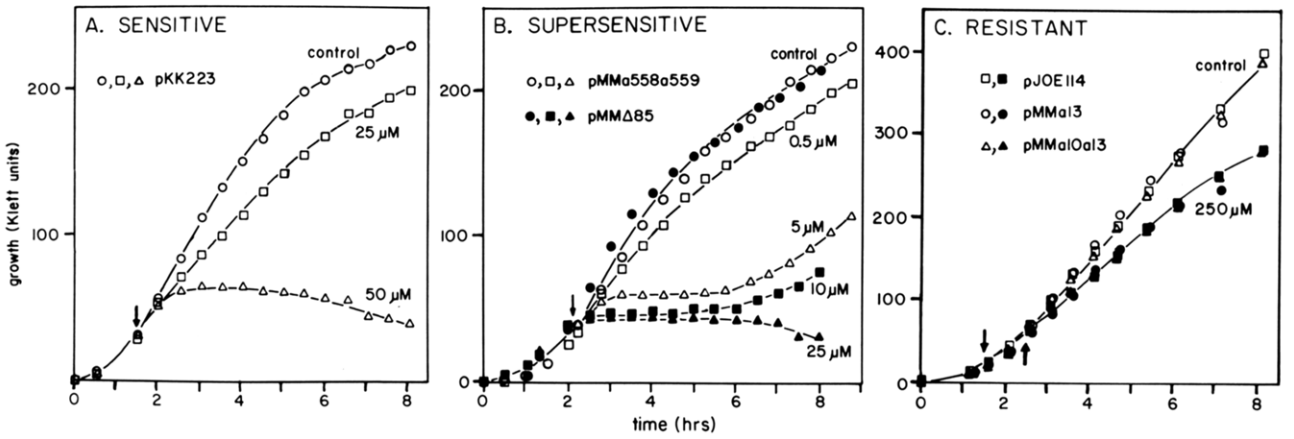

FIGURE 3: Growth curve assays for $HgCl_2$-sensitive (A), -supersensitive (B) or -resistant (C) phenotypes. HB101* cells containing the indicated plasmids were grown at 37 °C in 2 × YT liquid medium to approximately 35 Klett units of turbidity, when the cultures were divided and the indicated concentrations of $HgCl_2$ added (arrows). In (C) $HgCl_2$ was first added to 50 μM, and then after 1 h of induction the concentration was boosted to 250 μM total (see Discussion). Controls contained no $HgCl_2$. pKK223 has no *mer* genes, while pJOE114 contains the wild-type Tn*501 mer* operon. pMMa558a559, pMMΔ85, pMMa13, and pMMa10a13 are pJOE114 variants encoding the mutant mercuric reductases described in the text.

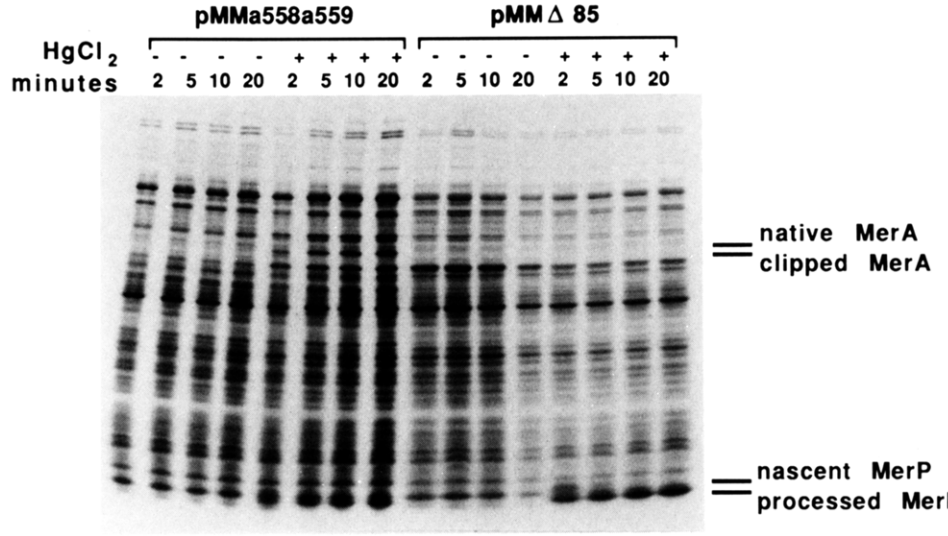

FIGURE 4: Pulse labeling of $HgCl_2$-induced proteins encoded by pMMa558a559 and pMMΔ85. Cultures were grown (see Methods) to A_{550} = 0.43, and 0.5 μM $HgCl_2$ was added to half of each. After 15 min, [^{35}S]cysteine and [^{35}S]methionine were each added to 10 μCi/mL, and 1-mL samples were removed at 2, 5, 10, and 20 min thereafter. Cells were pelleted and flash frozen to halt metabolism, and then total cell protein was electrophoresed on a denaturing 5–20% polyacrylamide gradient gel. Presence or absence of $HgCl_2$ induction is indicated by (+) and (−), while the bars indicate the molecular weights of expected protein products.

centrations (data not shown). For each mutant there are four possible scenarios that would result in the above observations: (1) the mutant *merA* gene is not effectively translated, (2) the polypeptide is synthesized but does not fold properly, (3) the polypeptide is synthesized but is proteolytically labile, or (4) the mutant protein is structurally intact but catalytically impaired.

To differentiate among these possibilities, the $HgCl_2$-inducible translation products of both plasmids were examined via [^{35}S]cysteine/methionine pulse labeling. The resulting autoradiograph is shown in Figure 4. Upon induction with 0.5 μM $HgCl_2$, both pMMΔ85 and pMMa558a559 clearly encode polypeptide bands of the correct molecular mass for nascent (9-kDa) and periplasmic (7.5-kDa) MerP, indicating that *mer* operon induction has occurred. [Jackson and Summers (1982) have shown that MerT is present at significantly lower levels than MerA and MerP and thus cannot be seen in this total cell protein gel.] However, while pMMa558a559 also encodes a distinct protein band of identical molecular mass to wild-type mercuric reductase (59 kDa), no such band can be seen, either visually or by scanning laser densitometry, from pMMΔ85 corresponding to the N-terminal-deleted or "clipped" form of the enzyme (50 kDa). Clipped mercuric reductase retains 14 of the 18 cysteines and methionines found per subunit of the $Ala_{558}Ala_{559}$ protein, putting the lower detection limit for densitometry detection of clipped protein at ca. 6% of the level of the $Ala_{558}Ala_{559}$ enzyme (data not shown). Lastly, over the time course of this experiment, there is no significant decrease in the intensity of the $Ala_{558}Ala_{559}$ 59-kDa protein band, indicating that this mutant protein is not particularly sensitive to proteolysis.

In summary, the above results show that the $Ala_{558}Ala_{559}$ mutation must result in either an incorrectly folded protein or a catalytically incapacitated enzyme, while deletion of the codons for residues 2–86 of *merA* results in a very significant decrease in protein expression.

$Ala_{558}Ala_{559}$ Mercuric Reductase Overproduction and Purification. To facilitate purification, the $Ala_{558}Ala_{559}$ mutant *merA* gene was cloned behind the *tac* promotor of plasmid pSE181 as shown in Figure 2. This construction, pMMOa558a559, differs from the wild-type and mutant mercuric reductase overproducing plasmids described by

Schultz et al. (1985) in that only the 1861 bp *Aha*II fragment of pMMa558a559 (containing the $Ala_{558}Ala_{559}$ mutant *merA* gene and the beginning of *merD*) was inserted into the pSE181 vector. In contrast, pPSO1, the wild-type enzyme overproducing plasmid, was constructed by using a much larger, 3551 bp *Nar*I/*Pvu*II pJOE114 fragment as the insert into pSE181. pMMOa558a559 directs the overproduction of $Ala_{558}Ala_{559}$ mercuric reductase to >6.5% total soluble protein as determined by transhydrogenase activity in crude cell extracts (data not shown). For comparison, pPSO1 directs the overproduction of wild-type mercuric reductase to 5% total soluble protein (Schultz et al., 1985).

$Ala_{558}Ala_{559}$ mercuric reductase was isolated in >100-mg quantities via a one-step purification using Orange A affinity chromatography. This purification scheme has been used previously for the wild-type protein as well as all of the redox-active disulfide mutants (Fox & Walsh, 1982; Schultz et al., 1985; Distefano et al., 1989). Since binding of the protein to Orange A and its elution with NADPH presumably depend on an intact nicotinamide binding site, the success of this affinity chromatography step implied that the $Ala_{558}Ala_{559}$ mutant protein is properly folded and is functional for NADPH binding.

Thiol Titrations. The thiol content of KBr-dialyzed $Ala_{558}Ala_{559}$ protein in the absence or presence of excess NADPH was determined with DTNB as described by Riddles et al. (1983). Upon denaturation with 6 M guanidine hydrochloride, 2.1 and 3.9 thiols were titrated, respectively. This increase of two thiols upon NADPH addition confirms the presence of an intact redox-active disulfide in the $Ala_{558}Ala_{559}$ enzyme. Titrations performed in 4–5 M guanidine hydrochloride, as described by Schultz et al. (1985) for the active site mutants, consistently resulted in a difference of ca. 1.3 thiols between oxidized and reduced $Ala_{558}Ala_{559}$ enzyme, possibly due to incomplete protein denaturation. When we denatured the wild-type enzyme in 6 M guanidine hydrochloride, 2.1 and 4.8 thiols were titrated in its oxidized and NADPH-reduced forms. This is consistent with both complete reduction of the redox-active disulfide and partial reduction of a second disulfide, as discussed in the following paper (Miller et al., 1989).

Physical Properties. $Ala_{558}Ala_{559}$ mercuric reductase exhibits many of the same physical properties as the wild-type enzyme. Both $Ala_{558}Ala_{559}$ and wild-type proteins when freshly isolated migrate with an apparent subunit molecular mass of 59 kDa on 9% SDS–polyacrylamide gels. However, over time (1–4 weeks) both proteins become increasingly clipped, perhaps via a minimal protease contaminant, and migrate with an apparent molecular mass of 50 kDa. Fox and Walsh (1983) showed that this clipping results in the removal of an 85 amino acid N-terminal domain, but that clipped wild-type enzyme does not differ catalytically from unclipped enzyme.

The native molecular masses of both the mutant and wild-type enzymes are somewhat ambiguous when determined by gel chromatography; they elute as single peaks between the elution volumes expected for dimeric and trimeric holoenzymes (i.e., between 120 and 180 kDa). Evidence for both dimeric and trimeric mercuric reductases has been previously reported (Fox & Walsh, 1982; Rinderle et al., 1983; Schottel, 1978), although given its homology with the other disulfide oxidoreductases, it has been assumed that the biologically relevant structure is a dimer. In the present study, we observe that older enzyme samples that have become clipped behave more like dimeric species by gel chromatography, while unclipped samples behave more like trimers (data not shown). These results suggest that mercuric reductase is indeed a dimer with the N-terminal domain making the protein less globular (S. Silver, personal communication), i.e., of a seemingly higher molecular mass, and are consistent with results of Rinderle et al. (1983), who observed that clipped samples of R100 mercuric reductase also exhibit dimeric native molecular mass.

The spectral ratio A_{272}/A_{456} is 6.3 for both the wild-type and the $Ala_{558}Ala_{559}$ mutant, corresponding to a maximal flavin loading of 1 FAD per protein monomer (Fox & Walsh, 1983). In contrast to some of the redox-active disulfide mutants (Distefano et al., 1989), no significant flavin loss was observed in this mutant even after prolonged dialysis, indicating that there is little or no disruption of the FAD binding domain caused by the $Ala_{558}Ala_{559}$ mutation.

Spectroscopic Properties and Electron Capacity. Like other oxidoreductases of this class, in the absence of nicotinamide adenine dinucleotides, wild-type mercuric reductase can exist in three *spectrally distinct* redox states (Fox & Walsh, 1982): (1) fully oxidized (E_{ox} = oxidized flavin and redox-active disulfide), characterized by an absorbance maximum at 456 nm (ϵ = 11.3 mM^{-1} cm^{-1}), (2) two electron reduced (EH_2 = oxidized flavin and redox-active dithiol), possessing a long-wavelength charge-transfer absorbance from interaction of the Cys_{140} thiolate with oxidized flavin, and (3) four electron or fully reduced (EH_4 = reduced flavin and redox-active dithiol) that exhibits a bleached spectrum due to reduction of the FAD prosthetic group.

Figure 5A shows a redox titration of the $Ala_{558}Ala_{559}$ mutant protein. From this figure it can be seen that, unlike the active site mutants described by Distefano et al. (1989) and Schultz et al. (1985), the visible spectra of the $Ala_{558}Ala_{559}$ enzyme are remarkably similar to those of the wild-type enzyme. [Wild-type spectra are not shown in Figure 5 for the sake of simplicity, but may be found in the following paper (Miller et al., 1989)]. In fact, the E_{ox} spectra of the two are superimposable with the same absorbance maximum of 456 nm and extinction coefficient of 11.3 mM^{-1} cm^{-1}. Similarly, as the $Ala_{558}Ala_{559}$ enzyme is titrated with dithionite, it progresses through the same set of spectral changes as does the wild type, with their respective EH_2 and EH_4 spectra again superimposable. The EH_2 flavin absorbance maximum for both is 438 nm (ϵ = 8.6 mM^{-1} cm^{-1}), while the charge-transfer absorbance maximum for both is 540 nm (ϵ = 2.6 mM^{-1} cm^{-1}). By plotting A_{540} vs electron equivalents added (Figure 5A, inset), we see that full charge-transfer absorbance (EH_2) develops after addition of 1.6 electron equiv and that the enzyme is fully reduced to EH_4 upon the input of another 2.3 electron equiv. We also note that the 2 electron equiv lag observed upon titration of the wild type before its oxidized spectrum begins to change (Fox & Walsh, 1983; Miller et al., 1989) is totally absent from the $Ala_{558}Ala_{559}$ titration. Thus, $Ala_{558}Ala_{559}$ mercuric reductase has a total redox capacity of 4 electrons.

A titration of $Ala_{558}Ala_{559}$ mercuric reductase with NADPH, the enzyme's physiological reductant, is shown in Figure 5B. Much like its behavior upon titration with dithionite, we again see this mutant proceed through the same set of equilibrium charge-transfer species as the wild-type enzyme. The first of these is an EH_2-$NADP^+$ complex, which exhibits a blue-shifted flavin absorbance maximum at 448 nm (ϵ = 8.0 mM^{-1} cm^{-1}) and a charge-transfer absorbance band centered around 560 nm (ϵ = 3.0 mM^{-1} cm^{-1}). Further addition of NADPH leads to the formation of an EH_2–NADPH complex whose flavin and charge-transfer absorbances are centered at 444 nm (ϵ = 8.6 mM^{-1} cm^{-1}) and 530 nm (ϵ = 4.9 mM^{-1} cm^{-1}), respectively. As can be seen from the following paper

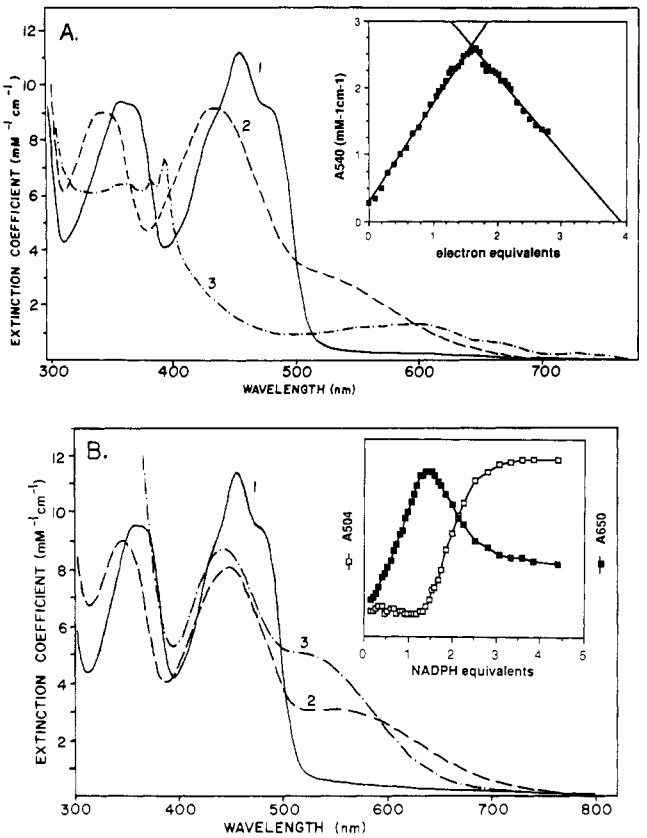

FIGURE 5: Dithionite and NADPH titrations of $Ala_{558}Ala_{559}$ mercuric reductase. KBr-dialyzed samples were made anaerobic and titrated with dithionite or NADPH as described under Methods. Spectra shown in (A) are of enzyme samples in the presence of (1) 0.0 (E_{ox}), (2) 1.60 (EH_2), and (3) 3.30 (EH_4) equiv of dithionite. (Spectrum 3 contains some absorbance from reduced methylviologen, which was added to the titration as a mediator.) Part A insert follows charge-transfer absorption, A_{540}, as a function of equivalents of dithionite/enzyme monomer. Part B shows the spectra of enzyme in the presence of (1) 0.0 (E_{ox}), (2) 1.3 equiv (EH_2–NADP$^+$), and (3) 5.0 equiv (EH_2–NADPH) of NADPH, while the inset follows A_{504} (isosbestic point for the E_{ox} to EH_2–NADP$^+$ transition) and A_{650} (indicative of changes from E_{ox} to EH_2–NADP$^+$ to EH_2–NADPH) as a function of equivalents of NADPH/enzyme monomer.

(Miller et al., 1989), the spectra observed in this titration closely match those obtained with the wild-type enzyme. However, the wild-type and $Ala_{558}Ala_{559}$ enzymes do differ significantly in the number of NADPH equivalents each requires for formation of the two complexes. Miller et al. show that, at 25 °C, equilibrium EH_2–NADP$^+$ formation by the wild-type enzyme requires 2 equiv of NADPH, while EH_2–NADPH is fully formed only when NADPH is present in greater than a 10 molar excess. In contrast, as shown in Figure 5B, inset, the $Ala_{558}Ala_{559}$ enzyme takes up only 1.1 equiv of NADPH to form a stable EH_2–NADP$^+$ complex, and EH_2–NADPH formation is complete with only 3.3 total equiv of NADPH.

The fact that the $Ala_{558}Ala_{559}$ mutation produces no significant perturbations in the visible absorbance spectra of the various oxidized and reduced mercuric reductase species indicates that, compared to Cys_{135} and Cys_{140}, the C-terminal cysteines are not in intimate contact with the flavin. Yet, given the effect of this mutation on the enzyme's $Hg(SR)_2$ reductase activity (see below), it seemed likely that Cys_{558} and/or Cys_{559} is located within the active site and may thus have an effect on the FAD fluorescence spectrum. However, the fluorescence properties of the E_{ox} forms of both enzymes are quite similar, both having excitation and emission maxima at 4 °C of 455 and 520 nm, respectively (data not shown). In fact, the only significant differences in the fluorescence spectra of the two enzymes are their respective intensities when compared to that of free FAD in solution. These data are presented and discussed in detail in the following paper (Miller et al., 1989).

Redox Potentials. We have previously reported E_{ox}/EH_2 and EH_2/EH_4 midpoint potentials for wild-type mercuric reductase to be −269 and −335 mV, respectively (Fox & Walsh, 1982). The E_{ox}/EH_2 value was determined via dithionite titration in the presence of the redox dyes 1-deazariboflavin and phenosafrarin, while the EH_2/EH_4 couple was obtained by measuring the amount of disproportionation of EH_2 to yield E_{ox} and EH_4 at various pH values.

In the current work we have exploited a continuously reducing xanthine/xanthine oxidase system developed by Dr. Vincent Massey for determining midpoint potentials [see footnote 2, Distefano et al. (1989)]. From separate titrations using either 1-deazariboflavin ($E^{\circ\prime}$ = −280 mV) or benzylviologen ($E^{\circ\prime}$ = −358 mV) as indicator dye, we determined the E_{ox}/EH_2 potential of the $Ala_{558}Ala_{559}$ enzyme to be −310 or −292 mV, respectively (average = −300 mV). Plots of E_{obsd} vs log (E_{ox}/EH_2) for each case gave slopes of 29 and 31 mV, respectively, confirming the two-electron nature of this reduction. We also used benzylviologen as the indicator for the EH_2/EH_4 potential determination. Reduction from EH_2 to EH_4, however, is clearly a complicated process as evidenced by the distinct biphasicity of the E_{obsd} vs log (EH_2/EH_4) plot (data not shown). The first half of the reduction [i.e., log (EH_2/EH_4) > 0] yields a slope of 68 mV and midpoint potential of −348 mV, while the second half [log (EH_2/EH_4) < 0] has a slope of 32 mV and the midpoint potential of −351 mV. Such evidence for two categories of reduction sites was first observed by V. Massey with the $Cys_{135}Ser_{140}$ and $Ser_{135}Cys_{140}$ mutant enzymes and will be fully addressed in a later paper (V. Massey et al., unpublished results).

Enzymatic Activities. We have assayed three aerobic and two anaerobic catalytic activities for the $Ala_{558}Ala_{559}$ and wild-type mercuric reductases. The aerobic activities are $Hg(SR)_2$-independent NADPH oxidation (O_2 reduction), NADPH/thio-NADP$^+$ transhydrogenation, and $Hg(SR)_2$-dependent NADPH oxidation. The anaerobic activities are DTNB reduction and $Hg(SR)_2$ reduction via $^{203}Hg(0)$ volatilization. The results of these assays are summarized in Tables II and III. Except where noted, wild-type catalytic parameters were determined in parallel with those of the mutant both to serve as a control and to confirm previous results. All rates are expressed as the rate per enzyme monomer.

O_2 Reduction. In all activities tested not involving Hg(II), the $Ala_{558}Ala_{559}$ enzyme is again remarkably similar to wild-type mercuric reductase. For example, under aerobic conditions both enzymes have a $Hg(SR)_2$-independent NADPH oxidase activity: with 200 μM NADPH and air-saturated buffer (37 °C), they both catalyze the production of H_2O_2 at a rate of 2 min^{-1}. This rate was determined both by NADPH consumption (decrease of A_{340}) and by O_2 consumption (oxygen electrode). Schultz et al. (1985) have shown previously, via catalase addition, that the product of this activity is indeed H_2O_2.

Transhydrogenation. Both wild-type and mutant enzymes also catalyze the transhydrogenation of thio-NADP$^+$ and NADPH. This activity allows the determination of a K_m for NADPH (in 100 μM thio-NADP$^+$), which is 0.71 μM for the $Ala_{558}Ala_{559}$ enzyme and 0.8 μM for the wild type (Schultz et al., 1985). The k_{cat} for transhydrogenation (25 °C) is 116 min^{-1} for the $Ala_{558}Ala_{559}$ mutant, representing a 2-fold rate

Table II: Catalytic Activities of Wild-Type and $Ala_{558}Ala_{559}$ Mercuric Reductases

activity	conditions and parameter monitored	wild type	$Ala_{558}Ala_{559}$
transhydrogenation	aerobic, 25 °C NADPH consumption	K_m = 0.8 μM NADPH[a] k_{cat} = 46 min^{-1}	K_m = 0.71 μM NADPH k_{cat} = 116 min^{-1}
NADPH oxidation/O_2 reduction	aerobic, 37 °C O_2 or NADPH consumption	TN = 2.0 min^{-1} [b]	TN = 2.0 min^{-1}
DTNB reduction	anaerobic, 25 °C TNB^- production	K_m = 1.4 mM DTNB k_{cat} = 102 min^{-1} K_{si} = 7.0 mM DTNB	K_m = 1.2 mM DTNB k_{cat} = 132 min^{-1} K_{si} = 5.9 mM DTNB
$Hg(SR)_2$-stimulated NADPH oxidation	aerobic, 37 °C NADPH consumption	K_m = 5.0 μM $HgCl_2$ k_{cat} = 810 min^{-1}	K_m = 45 μM $HgCl_2$ k_{cat} = 6.6 min^{-1}
$Hg(SR)_2$-stimulated NADPH oxidation	aerobic, 37 °C O_2 consumption	ND	K_m = 88 μM $HgCl_2$ k_{cat} = 8.2 min^{-1}

[a] Fox & Walsh, 1982. [b] Rates are expressed as turnover numbers (TN) if the rate was only examined under one set of conditions (i.e., neither substrate concentration was varied). k_{cat} indicates an apparent k_{cat}; i.e., the concentration of only one substrate was varied, while the other was kept constant.

enhancement over that of wild-type enzyme. In this aspect the mutant resembles the Cys_{135}-alkylated wild-type enzyme, which has a 2.5–6-fold higher transhydrogenase k_{cat} than its nonalkylated form (Fox & Walsh, 1983).

DTNB Reduction. Schultz et al. (1985) previously reported that the wild-type and $Cys_{135}Ser_{140}$ mutant enzymes can catalytically reduce the aryl disulfide 5,5′-dithiobis(2-nitrobenzoate) (DTNB) in an activity analogous to the thiol/disulfide interchange reactions catalyzed by the other members of this enzyme family. They reported K_m and k_{cat} values for the wild-type enzyme of 0.4 mM DTNB and 220 min^{-1}, respectively. However, Au (1986) subsequently reported that the 220-min^{-1} value for k_{cat} was not reproducible. Thus we decided to reexamine the reduction of DTNB by wild-type mercuric reductase, as well as determine kinetic parameters for the $Ala_{558}Ala_{559}$ mutant. All DTNB reduction assays were conducted in anaerobic solutions with 200 μM NADPH as described under Methods. Under these conditions, we have observed two previously unreported phenomena: (1) an NADPH- and DTNB-dependent enzyme activation and (2) a second-site DTNB-dependent inhibition. The activation results in biphasic kinetics with an initial slow TNB production phase being replaced by a faster linear rate over a period of 2–8 min. Both the amount of activation and the time required to reach the linear rate were dependent on [DTNB] with 5 mM and above giving a 4.5-fold activation after 6–8 min. The activation was not affected by prior incubation of the enzyme with either NADPH or DTNB alone and thus requires the presence of both substrates. The second phenomenon, that of a second inhibitory binding site for DTNB, is evidenced by a nonlinear [DTNB] vs [DTNB]/v plot above 5 mM DTNB. Using the faster, linear rates of TNB production described above, we have determined K_m, k_{cat}, and K_{si} values (Cornish-Bowden, 1981) for the wild type to be 1.4 mM DTNB, 103 min^{-1}, and 7.0 mM DTNB, respectively. The $Ala_{558}Ala_{559}$ enzyme is quite similar, with a K_m of 1.2 mM DTNB, k_{cat} of 132 min^{-1}, and K_{si} of 5.9 mM DTNB.

Aerobic $Hg(SR)_2$-Dependent NADPH Oxidation. While the $Ala_{558}Ala_{559}$ mutant appears to be very like the wild type in its catalysis of the above Hg(II)-independent reactions, examination of its behavior upon addition of $Hg(SR)_2$ reveals that it is quite different in its ability to handle and reduce Hg(II). Under aerobic conditions, Fox and Walsh (1982) showed that the wild-type enzyme exhibits biphasic consumption of NADPH upon $Hg(SR)_2$ addition, with an initial fast phase giving a k_{cat} of 810 min^{-1} and a slower, nearly linear phase giving a k_{cat} of 340 min^{-1}. Using the faster phase, we found that for wild-type enzyme, the K_m for Hg(II) in the presence of 1 mM β-mercaptoethanol is 5.0 μM, consistent with the value of 12 μM reported by Fox and Walsh (1982). In contrast, under the same conditions the $Ala_{558}Ala_{559}$ mutant exhibits only a linear rate of NADPH consumption with a k_{cat} of 6.6 min^{-1} and K_m of 45 μM $Hg(SR)_2$. Interestingly, Schultz and co-workers (1985) observed almost identical kinetic parameters (k_{cat} = 6.5 min^{-1}, K_m = 48 μM) for the $Ser_{135}Cys_{140}$ mutant with $Hg(CN)_2$. Recently, Distefano et al. (1989) have shown this NADPH consumption to result from a saturable increase in the NADPH-dependent O_2-reduction rate rather than from Hg(II) turnover. In light of this, we also examined the effects of $Hg(SR)_2$ on the O_2 consumption rate of the $Ala_{558}Ala_{559}$ mutant and likewise observed saturable kinetics with K_m = 88 μM $HgCl_2$ (in the presence of 1 mM β-mercaptoethanol) and k_{cat} = 8.2 min^{-1}. Thus, within experimental error, essentially all of the $Hg(SR)_2$-dependent NADPH consumption observed for the $Ala_{558}Ala_{559}$ mutant under aerobic conditions can be accounted for by an Hg(II)-effected increase in the oxidase activity.

Table III: ^{203}Hg Volatilization by Wild-Type and $Ala_{558}Ala_{559}$ Mercuric Reductases and Yeast Glutathione Reductase

	enzyme (μM)	turnover no.[a] (min^{-1})	rel rate	turnovers monitored
wild type	0.002	318	19875	42900
$Ala_{558}Ala_{559}$	1.0	0.28	18	76
	0.5	0.30	19	134
yeast GR	4.0	0.016	1	9
	1.0	0.035	2	25

[a] Linear least-squares fit through all points above 60 μM [^{203}Hg].

Anaerobic $^{203}Hg(0)$ Volatilization. The above evidence indicates that although the $Ala_{558}Ala_{559}$ mutation drastically alters the enzyme's ability to reduce Hg(II), it has little effect on its other activities. In fact, one could argue that the $Ala_{558}Ala_{559}$ mutant, by virtue of its aryl disulfide (DTNB) reduction activity coupled with its inability to handle Hg(II), is actually a truer member of the flavin disulfide oxidoreductase family than is wild-type mercuric reductase. If this is indeed the case, then one might expect that if the $Ala_{558}Ala_{559}$ enzyme retains any residual $Hg(SR)_2$ reducing ability, other members of this family might also have similar, adventitious levels of mercuric ion reductase activity.

We have investigated the above possibility using a sensitive, anaerobic $^{203}Hg(0)$ volatilization assay (Schottel, 1978; Distefano et al., 1989). With this assay, we tested the $Hg(SR)_2$ reducing ability of the wild-type and $Ala_{558}Ala_{559}$ mercuric reductases and yeast glutathione reductase. Typical volatilization curves for all three enzymes are shown in Figure 6, and the kinetic data are summarized in Table III. We have found that both the $Ala_{558}Ala_{559}$ mutant mercuric reductase and yeast glutathione reductase can reduce Hg(II), albeit at very low rates. The former catalyzes Hg(0) evolution 1000-fold slower than wild-type mercuric reductase while the latter is 10-fold slower still. That these slow volatilizations were

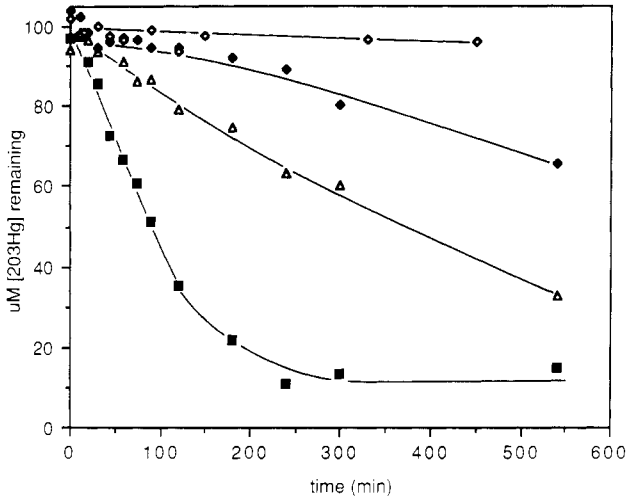

FIGURE 6: $^{203}Hg(0)$ volatilization curves for wild-type and $Ala_{558}Ala_{559}$ mercuric reductases and yeast glutathione reductase. Evolution of $^{203}Hg(0)$ from anaerobic assay mixtures containing 400 μM NADPH, 1 mM cysteine, and 100 μM $^{203}HgCl_2$ was followed as described under Methods. The volatilization curves shown are those for assay mixtures containing no enzyme (◇), 4.0 μM yeast glutathione reductase (◆), 0.5 μM $Ala_{558}Ala_{559}$ mercuric reductase (△), and 2 nM wild-type mercuric reductase (■).

enzyme catalyzed was confirmed by showing that the rates changed with enzyme concentration (Table III) and by following $^{203}Hg(0)$ evolution from a control assay mixture lacking enzyme (Figure 6).

Discussion

The main goal of this work has been to identify unique structural features of mercuric ion reductase that enable it to carry out the last step in the bacterial mercury detoxification pathway, i.e., reduction of Hg(II) to Hg(0). We have approached this problem by using site-directed mutagenesis experiments specifically designed to address two standing hypotheses: (1) that the C-terminal cysteine pair, $Cys_{558}Cys_{559}$, thiols are involved in correct Hg(II) positioning in the enzyme's active site and (2) that the N-terminal cysteine pair, $Cys_{10}Cys_{13}$, thiols participate in intracellular Hg(II) transport (Brown et al., 1983).

The first hypothesis was based on both molecular modeling studies and previous evidence that the C-terminal cysteine pair, $Cys_{558}Cys_{559}$ (Tn*501* mercuric reductase has 561 residues total), has access to the enzyme's active site. Chemical modification experiments by Fox and Walsh (1983) showed that if [^{14}C]iodoacetamide, a sulfhydryl-specific labeling reagent, is incubated with oxidized mercuric reductase, no label is incorporated into the protein. However, if mercuric reductase is previously reduced with dithionite to the EH_2 state, iodoacetamide is incorporated with a stoichiometry of 1 iodoacetamide/monomer, and 20% of this label is found in the C-terminal peptide. By modeling the amino acid sequence of mercuric reductase onto the 2.0-Å crystal structure of glutathione reductase (no such structure currently exists for mercuric reductase), Brown et al. (1983) suggested that this cysteine pair may be involved in Hg(II) binding at the active site of the opposite subunit.

In the current study, we have constructed an $Ala_{558}Ala_{559}$ mutant mercuric reductase and have shown that it encodes a supersensitive phenotype in vivo and that its catalytic competence for Hg(II) reduction in vitro has been reduced by ca. 1000-fold (Table III). The fact that this mutant is so similar physically and spectrally to the wild-type enzyme and that it catalyzes NADPH oxidation, transhydrogenation, and DTNB reduction with kinetic parameters so similar to those of wild type suggests that much of the active site residue alignment must be unchanged. The key observation that only Hg(II) reduction is differentially affected singles out Cys_{558} or Cys_{559} or both as crucial components for either Hg(II) coordination or electron transfer during catalysis. The necessity for the C-terminal cysteines is also brought out by the fact that the $FAD/FADH_2$ redox potential for the $Ala_{558}Ala_{559}$ mutant (see below) is actually more favorable for Hg(II) reduction than is that of the wild type.

We have also shown that another member of the flavin disulfide oxidoreductase family, yeast glutathione reductase, possesses a very low, but detectable, level of mercuric ion reductase activity. [This finding is consistent with results from the preceding paper (Distefano et al., 1989) showing that even $FADH_2$ free in solution is capable of slowly reducing Hg(II).] It has long been proposed that mercuric reductase and glutathione reductase evolved from a common ancestral oxidoreductase [see Summers (1986)]. However, the key question of how substrate exclusivity developed between these two enzymes had not been previously addressed. The observation that removal of Cys_{558} and Cys_{559} from mercuric reductase results in a decrease in its Hg(II) reduction rate by 3 orders of magnitude, while the rest of this enzyme molecule contributes only a 10-fold increase in the same catalytic rate over glutathione reductase, indicates that the C-terminal cysteines are a major part of the answer. In line with this, the following paper (Miller et al., 1989) presents data showing that the redox state of the C-terminal cysteines has a dramatic effect on the Hg(II) reductase activity of the wild-type enzyme. Therein, hypotheses are presented for exactly how Cys_{558} and Cys_{559} might participate in catalysis.

Several lines of evidence have suggested that the N-terminal cysteine pair might be involved in a cytoplasmic Hg(II)-transport or -binding function: (1) the first 85 amino acids of mercuric reductase can be removed in vitro with no effect on catalytic activity (Fox & Walsh, 1983), yet this domain is conserved in three known mercuric reductases (Brown et al., 1983; Misra et al., 1985; Laddaga et al., 1987); (2) at the protein level, the N-terminal domain shows >30% sequence homology to MerP, the periplasmic Hg(II)-binding protein; and (3) MerP contains only two cysteines, Cys_{33} and Cys_{36}, that are found in a region having considerable homology to the sequences surrounding the $Cys_{10}Cys_{13}$ mercuric reductase pair (Summers, 1986).

The similarities between MerP and the N-terminal domain of mercuric reductase led Brown and Goddette (1984) to propose that *merA* may have arisen as the result of a gene duplication event that combined a primordial disulfide oxidoreductase gene with an ancestral *merP*. Brown (1985) has further hypothesized that mercuric reductase may transiently associate with the *merT* gene product at the cell membrane, with incoming Hg(II) being transferred from MerT to the $Cys_{10}Cys_{13}$ thiol pair. Under this model the Hg(II) would then be transferred to the $Cys_{558}Cys_{559}$ pair where it would be correctly positioned, with the $Cys_{135}Cys_{140}$ pair, for reduction. Thus the N-terminal domain of mercuric reductase would play a parallel role in the cytoplasm to that played by MerP in the periplasm.

Recent site-directed mutagenesis studies of the MerP $Cys_{33}Cys_{36}$ pair have shown that removal of either residue does indeed disrupt the normal functioning of the mercury detoxification pathway (Nancy Hamlett, personal communication). Cys to Gly mutants exhibit a Hg(II) resistance phenotype intermediate between wild-type resistance and background

sensitivity (i.e., the resistance phenotype of cells containing no *mer* genes). These results are in agreement with those expected for a *mer* operon encoding a working reductase but a nonfunctional transport system. Concordantly, Lund and Brown (1987) have recently shown that deletion of the transport genes, leaving *merA* intact, results in a similar phenotype.

From these observations, one might expect that if the $Cys_{10}Cys_{13}$ pair does indeed perform a Hg(II)-binding function as part of the transport system, Cys to Ala mutants would be less resistant to Hg(II). However, under the conditions employed here, we could see no difference in the conferred mercury resistance of the $Cys_{10}Ala_{13}$ and $Ala_{10}Ala_{13}$ mutants when compared to that of wild-type *mer* operon. Using a minimum inhibitory concentration assay, Brown and co-workers (personal communication) have been able to observe a small phenotypic difference between the $Cys_{10}Ala_{13}$ mutant and the wild type: If the cells are preinduced with low concentrations of $HgCl_2$ for 1–2 h and then tested for $HgCl_2$ resistance on agar plates, the $Cys_{10}Ala_{13}$ cells are slightly less resistant than the wild-type cells; without the preinduction no difference was observed. Currently, we do not know whether this small difference is due to a transport aberration or to a decrease in the overall number of cellular thiols to which ligation of Hg(II) is not deleterious.

One possible cause for the lack of observable phenotypic change is the fact that all of our in vivo assays have been performed using multiple-copy plasmids. Under these circumstances, induction of the *mer* operon produces much more protein than is necessary for resistance (Nakahara et al., 1979a) and may thus swamp out any small Hg(II)-transport perturbations. Ni'Bhriain et al. (1983) have previously noted a similar but opposite effect with Tn5 insertion mutations in the *merD* gene; i.e., such insertions confer Hg(II) sensitivity only when present on multiple-copy plasmids. Currently, Brown and co-workers are working to clone the $Cys_{10}Ala_{13}$ and $Ala_{10}Ala_{13}$ mutant *merA* genes onto single-copy plasmids to assess their in vivo effects under nonamplified conditions.

Given that mutation of the N-terminal cysteine pair has little or no effect on *mer* operon function, we decided to address more stringently the role of the entire N-terminal domain by examining the consequences of its complete removal in vivo. This was accomplished by simply looping out the DNA coding for residues 2–86, making Ala_{87} the second amino acid in the coding region. This gene, *merAΔ85*, retains all of the upstream sequences of wild-type *merA*, including its SD sequence and spacing. However, as shown under Results, this "clipped" gene is not efficiently translated and thus results in a Hg(II)-supersensitive phenotype. While we do not presently understand the reason for this phenomenon, a clue may be found in the sequence now immediately downstream from the ATG start codon. This sequence, *ATG*GCCGCCGCCGCC..., with its high GC content, may effectively inhibit translation initiation [for review see Stormo (1986)].

Summary. We have constructed four mutations in mercuric ion reductase to probe the function of its N- and C-terminal cysteine pairs in Hg(II) detoxification. In vivo resistance assays indicate that the N-terminal cysteines are not essential for $HgCl_2$ resistance while in vitro characterization of the $Ala_{558}Ala_{559}$ mutant enzyme has revealed a function for the C-terminal cysteines in catalysis. Additional studies with single Cys to Ala mutants of the C-terminal pair and/or hybrid mutants, e.g., a mixture of $Ala_{135}Ala_{140}$ and $Ala_{558}Ala_{559}$ subunits, may help to address the questions of placement of the four thiol side chains during Hg(II) reduction.

ACKNOWLEDGMENTS

We thank A. Summers, S. Miller, V. Massey, C. Williams, and D. Ballou for providing helpful insights and for reading preliminary copies of the manuscript. We thank V. Massey for determining fluorescence spectra and for providing details of his yet unpublished xanthine/xanthine oxidase system for determination of redox potentials. We also gratefully acknowledge M. Distefano, K. Au, P. Schultz, and other members of the Walsh group for their contributions.

Registry No. Cys, 52-90-4; Ala, 56-41-7; NADPH, 53-57-6; DTNB, 69-78-3; $HgCl_2$, 7487-94-7; mercuric ion reductase, 67880-93-7; mercury, 7439-97-6.

REFERENCES

Amersham (1983) *M13 Cloning and Sequencing Handbook*, Amersham Corp., Arlington Heights, IL.

Au, K. G. (1986) *Mechanistic Studies of Active Site Mutants of Mercuric Reductase; Stereochemical Studies of a Fluoroacetate Halidohydrolase* (Ph.D. thesis) MIT, Cambridge, MA.

Biosearch (1984) *SamI Operator's Manual*, Biosearch, San Rafael, CA.

Brown, N. L. (1985) *Trends Biochem. Sci. 10*, 400–403.

Brown, N. L., & Goddette, D. (1984) in *Flavins and Flavoproteins* (Bray, R. C., Engel, P. C., & Mayhew, S. G., Eds.) pp 165–168, de Gruyter, Berlin.

Brown, N. L., Ford, S. J., Pridmore, R. D., & Fritzinger, D. C. (1983) *Biochemistry 22*, 4089–4095.

Casola, L., & Massey, V. (1966) *J. Biol. Chem. 241*, 4985–4993.

Cornish-Bowden, A. (1981) *Fundamentals of Enzyme Kinetics*, pp 93–95, Butterworths, Boston, MA.

Distefano, M. D., Au, K. G., & Walsh, C. T. (1989) *Biochemistry* (preceding paper in this issue).

Foster, T. J. (1983) *Microbiol. Rev. 47*, 361–409.

Fox, B., & Walsh, C. T. (1982) *J. Biol. Chem. 257*, 2498–2503.

Fox, B. S., & Walsh, C. T. (1983) *Biochemistry 22*, 4082–4088.

Hames, B. D. (1981) in *Gel Electrophoresis of Proteins: A Practical Approach* (Hames, B. D., & Rickwood, D., Eds.) IRL Press, Washington, DC.

Hanahan, D. (1985) in *DNA Cloning: A Practical Approach* (Clover, D. M., Ed.) Vol. I, IRL Press Ltd., Oxford, England.

Jackson, W. J., & Summers, A. O. (1982) *J. Bacteriol. 151*, 962–970.

Kunkel, T. A. (1985) *Proc. Natl. Acad. Sci. U.S.A. 82*, 488–492.

Kunkel, T. A. (1988) *Methods Enzymol.* (in press).

Laddaga, R. A., Chu, L., Misra, K. T., & Silver, S. (1987) *Proc. Natl. Acad. Sci. U.S.A. 84*, 5106–5110.

Lund, P. A., & Brown, N. L. (1987) *Gene 52*, 207–214.

Maniatis, T., Fritsch, E. F., & Sambrook, J. (1982) *Molecular Cloning: A Laboratory Manual*, Cold Spring Harbor Laboratory, Cold Spring Harbor, NY.

Massey, V., & Williams, C. H., Jr. (1965) *J. Biol. Chem. 240*, 4470–4480.

Messing, J. (1983) *Methods Enzymol. 101*, 20–79.

Miller, S. M., Ballou, D. P., Massey, V., Williams, C. H., Jr., & Walsh, C. T. (1986) *J. Biol. Chem. 261*, 8081–8084.

Miller, S. M., Moore, M. J., Massey, V., Williams, C. H., Jr., Distefano, M. D., Ballou, D. P., & Walsh, C. T. (1989) *Biochemistry* (following paper in this issue).

Misra, T. K., Brown, N. L., Fritzinger, D. C., Pridmore, R. D., Barnes, W. M., Haberstroh, L., & Silver, S. (1984)

Proc. Natl. Acad. Sci. U.S.A. 81, 5975-5979.
Misra, T. K., Brown, N. L., Haberstroh, L., Schmidt, A., Goddette, D., & Silver, S. (1985) *Gene 34*, 253-262.
Nakahara, H., Kinscherf, T. G., Silver, S., Miki, T., Easton, A. M., & Rownd, R. H. (1979a) *J. Bacteriol. 138*, 284-287.
Nakahara, H., Silver, S., Miki, T., & Rownd, R. H. (1979b) *J. Bacteriol. 140*, 161-166.
Ni'Bhriain, N. N., Silver, S., & Foster, T. L. (1983) *J. Bacteriol. 155*, 690-703.
O'Halloran, T. V., & Walsh, C. T. (1987) *Science 235*, 211-214.
Riddles, P. W., Blakeley, R. L., & Zerner, B. (1983) *Methods Enzymol. 91*, 49-60.
Rinderle, S. J., Booth, J. E., & Williams, J. W. (1983) *Biochemistry 22*, 869-876.
Schottel, J. L. (1978) *J. Biol. Chem. 253*, 4341-4349.
Schultz, P. G., Au, K. G., & Walsh, C. T. (1985) *Biochemistry 24*, 6840-6848.
Seidman, M. (1985) *BMBiochemica 2(5)*, 10.
Shames, S. L., Fairlamb, A. H., Cerami, A., & Walsh, C. T. (1986) *Biochemistry 25*, 3519-3526.
Stanisich, V. A., Bennett, P. M., & Richmond, M. H. (1977) *J. Bacteriol. 129*, 1227-1233.
Stormo, G. D. (1986) in *Maximizing Gene Expression* (Reznikoff, W., & Gold, L., Eds.) pp 195-224, Butterworths, Stoneham, MA.
Summers, A. O. (1986) *Annu. Rev. Microbiol. 40*, 607-634.
Walsh, C., Fisher, J., Spencer, R., Graham, D. W., Ashton, W. T., Brown, J. E., Brown, R. D., & Rogers, E. F. (1978) *Biochemistry 17*, 1942-1951.
Williams, C. H., Jr., Arscott, D. L., Matthews, R. G., Thorpe, C., & Wilkinson, K. D. (1979) *Methods Enzymol. 62D*, 185-198.
Wilson, G. S. (1978) *Methods Enzymol. 54*, 396-410.
Zoller, M. J., & Smith, M. (1983) *Methods Enzymol. 100*, 468-500.

Evidence for the Participation of Cys_{558} and Cys_{559} at the Active Site of Mercuric Reductase†

Susan M. Miller,*,‡ Melissa J. Moore,§ Vincent Massey,‡ Charles H. Williams, Jr.,‡,∥ Mark D. Distefano,§ David P. Ballou,‡ and Christopher T. Walsh§

Department of Biological Chemistry, University of Michigan, Ann Arbor, Michigan 48109, Department of Biological Chemistry and Molecular Pharmacology, Harvard Medical School, Boston, Massachusetts 02115, and Veterans Administration Medical Center, Ann Arbor, Michigan 48105

Received June 1, 1988; Revised Manuscript Received September 20, 1988

ABSTRACT: Mercuric reductase, with FAD and a reducible disulfide at the active site, catalyzes the two-electron reduction of Hg(II) by NADPH. Addition of reducing equivalents rapidly produces a spectrally distinct EH_2 form of the enzyme containing oxidized FAD and reduced active site thiols. Formation of EH_2 has previously been reported to require only 2 electrons for reduction of the active site disulfide. We present results of anaerobic titrations of mercuric reductase with NADPH and dithionite showing that the equilibrium conversion of oxidized enzyme to EH_2 actually requires 2 equiv of reducing agent or 4 electrons. Kinetic studies conducted both at 4 °C and at 25 °C indicate that reduction of the active site occurs rapidly, as previously reported [Sahlman, L., & Lindskog, S. (1983) *Biochem. Biophys. Res. Commun. 117*, 231-237]; this is followed by a slower reduction of another redox group via reaction with the active site. Thiol titrations of denatured E_{ox} and EH_2 enzyme forms show that an additional disulfide is the group in communication with the active site. [^{14}C]Iodoacetamide labeling experiments demonstrate that the C-terminal residues, Cys_{558} and Cys_{559}, are involved in this disulfide. The fluorescence, but not the absorbance, of the enzyme-bound FAD was found to be highly dependent on the redox state of the C-terminal thiols. Thus, E_{ox} with Cys_{558} and Cys_{559} as thiols exhibits less than 50% of the fluorescence of E_{ox} where these residues are present as a disulfide, indicating that the thiols remain intimately associated with the active site. Initial velocity measurements show that the auxiliary disulfide must be reduced before catalytic Hg(II) reduction can occur, consistent with the report of a preactivation phenomenon with NADPH or cysteine [Sandstrom, A., & Lindskog, S. (1987) *Eur. J. Biochem. 164*, 243-249]. A modified minimal catalytic mechanism is proposed as well as several chemical mechanisms for the Hg(II) reduction step.

Mercuric reductase (MR)[1] plays a crucial role in bacterial detoxification of mercurials as it catalyzes the $2e^-$ reduction of Hg(II) shown in eq 1. The enzyme exhibits extensive similarities to the pyridine nucleotide disulfide oxidoreductases, lipoamide dehydrogenase and glutathione reductase, both in primary sequence and in spectral properties. Thus, they all

$$Hg(SR)_2 + NADPH + H^+ \rightarrow Hg^0 + NADP^+ + 2RSH \quad (1)$$

† This work was supported by National Institutes of Health Grants GM 11106 (V.M.), GM 21444 (C.H.W.), GM 20877 (D.P.B.), and GM 21643 (C.T.W.). M.J.M. is an NSF predoctoral fellow.

* To whom correspondence should be addressed.
‡ University of Michigan.
§ Harvard Medical School.
∥ Veterans Administration Medical Center.

[1] Abbreviations: DTNB, 5,5′-dithiobis(2-nitrobenzoic acid); DTT, dithiothreitol; E_{act}, mercuric reductase containing oxidized FAD and oxidized active site thiols, but reduced C-terminal thiols; EH_2, mercuric reductase containing oxidized FAD and the active site thiols reduced; EH_4, mercuric reductase containing $FADH_2$ and reduced active site thiols; E_{ox}, mercuric reductase containing oxidized FAD and active site disulfide; HPLC, high-performance liquid chromatography; MR, mercuric reductase; 4-PDS, 4,4′-dithiodipyridine; TPCK, *N*-tosyl-L-phenylalanine chloromethyl ketone.

0006-2960/89/0428-1194$01.50/0